J|A|C|S ARTICLES

Published on Web 11/19/2009

Copper−Metal Deposition on Self Assembled Monolayer for Making Top Contacts in Molecular Electronic Devices

Oliver Seitz,[†] Min Dai,[‡] F. S. Aguirre-Tostado,[†] Robert M. Wallace,[†] and Yves J. Chabal*[,†]

University of Texas at Dallas, Richardson, Texas 75080, and Rutgers University, Piscataway, New Jersey 08901

Received August 18, 2009; E-mail: chabal@utdallas.edu

Abstract: Molecular electronics is an attractive option for low-cost devices because it involves highly uniform self-assembly of molecules with a variety of possible functional groups. However, the potential of molecular electronics can only be turned into practical applications if reliable contacts can be established without damaging the organic layer or contaminating its interfaces. Here, a method is described to prepare tightly packed carboxyl-terminated alkyl self-assembled monolayers (SAMs) that are covalently attached to silicon surfaces and to deposit thin metallic copper top contact electrodes without damage to this layer. This method is based on a two-step procedure for SAM preparation and the implementation of atomic layer deposition (ALD) using copper di-*sec*-butylacetamidinate $[Cu(sBu\text{-}amd)]_2$. *In situ* and *ex situ* infrared spectroscopy (IRS), X-ray photoelectron spectroscopy (XPS), atomic force microscopy (AFM), and electrical measurements are used to characterize the chemical modification of the Si/SAM interface, the perturbation of the SAM layer itself, and the metal homogeneity and interaction with the SAM headgroups. This work shows that (i) carboxyl-terminated alkyl monolayers can be prepared with the same high density and quality as those achieved for less versatile methyl-terminated alkyl monolayers, as evidenced by electrical properties that are not dominated by interface defects; (ii) Cu is deposited with ALD, forming a bidentate complexation between the Cu and the COOH groups during the first half cycle of the ALD reaction; and (iii) the Si/SAM interface remains chemically intact after metal deposition. The nondamaging thin Cu film deposited by ALD protects the SAM layer, making it possible to deposit a thicker metal top contact leading ultimately to a controlled preparation of molecular electronic devices.

1. Introduction

Molecular and nanoscale electronics are driven by the technological need for low cost devices or ever decreasing dimensions and the scientific desire to understand nanoscale charge transport. Organic molecules are particularly interesting as nanoscale device elements because of the ability (i) to manipulate their functional groups by synthesis to satisfy varying technological requirements and (ii) to achieve atomic-scale uniformity using a self-assembly process. Ultimately, organic molecules may provide new options and functionality for low cost devices.[1,2]

However, these options and functionalities can only be turned into practical solutions if robust and reliable contacts can be established without damaging the organic layer or altering/contaminating the interfaces. Many approaches to establish electrical contacts have already been proposed and used for studying different systems. Haick and Cahen[3] and Akkerman and De Boer[4] have critically reviewed most of the methods developed for making contacts on self-assembled monolayers (SAMs) as well as single molecules, summarizing their approach and highlighting the advantages and limitations. In the case of the SAM layers, three basic methods of deposition have been used: (i) gentle deposition such as lift-off float-on (LOFO) and polymer assisted lift-off (PALO); in general, these approaches do not lead to homogeneous and intimate contact and result in poor reproducibility;[5−9] (ii) physical deposition such as metal evaporation, which forms homogeneous contacts but damages the organic layer[10−12] or leads to metal insertion within the organic layer;[13−16] and (iii) gentle and homogeneous deposition

[†] University of Texas at Dallas.
[‡] Rutgers University.

(1) Herwald, S. W.; Angello, S. J. *Science* **1960**, *132*, 1127–1133.
(2) Moore, G. E. *Electronics* **1965**, *38*, (April 19, 1965).
(3) Haick, H.; Cahen, D. *Prog. Surf. Sci.* **2008**, *83*, 217–261.
(4) Akkerman, H. B.; De Boer, B. *J. Phys.: Condens. Matter* **2008**, *20*.
(5) Vilan, A.; Cahen, D. *Adv. Funct. Mater.* **2002**, *12*, 795–807.
(6) Moons, E.; Bruening, M.; Shanzer, A.; Beier, J.; Cahen, D. *Synth. Met.* **1996**, *76*, 245–248.
(7) Shimizu, K. T.; Fabbri, J. D.; Jelincic, J. J.; Melosh, N. A. *Adv. Mater.* **2006**, *18*, 1499–1504.
(8) Vilan, A.; Ghabboun, J.; Cahen, D. *J. Phys. Chem. B* **2003**, *107*, 6360–6376.
(9) Vilan, A.; Shanzer, A.; Cahen, D. *Nature* **2000**, *404*, 166–168.
(10) Haick, H.; Niitsoo, O.; Ghabboun, J.; Cahen, D. *J. Phys. Chem. C* **2007**, *111*, 2318–2329.
(11) Lee, J. O.; Lientschnig, G.; Wiertz, F.; Struijk, M.; Janssen, R. A. J.; Egberink, R.; Reinhoudt, D. N.; Hadley, P.; Dekker, C. *Nano Lett.* **2003**, *3*, 113–117.
(12) Lioubtchenko, D. V.; Markov, I. A.; Briantseva, T. A. *Appl. Surf. Sci.* **2003**, *211*, 335–340.
(13) Nishizawa, M.; Sunagawa, T.; Yoneyama, H. *Langmuir* **1997**, *13*, 5215–5217.
(14) Oyamatsu, D.; Nishizawa, M.; Kuwabata, S.; Yoneyama, H. *Langmuir* **1998**, *14*, 3298–3302.

of metallic liquids (e.g., Hg), which is unfortunately not applicable for devices.[17−25]

These studies highlight the fact that control and understanding of the physical and electronic structure of molecules within the substrate (metal or semiconductor)−molecular-metal junctions remains extremely limited. This is especially true for molecules with reactive functional groups, where electronic or structural rearrangements may occur after top contact deposition. One of the primary challenges is to develop sample architectures that allow multiple analysis techniques to be brought to bear simultaneously to probe the structure before as well as after deposition of metals. Indeed, it is critical to be able to probe the packing and homogeneity of the SAMs, as well as the damage on the organic molecules and their interfaces after metal contact preparation.

In this study, a method is described to prepare thin metallic copper top contact electrodes on SAMs using atomic layer deposition (ALD), which has the potential to form metal layers with chemical bonds to the organic molecules. These intermediate thin protective and nondamaging metal layers can then be used as seed for deposition of a thicker metal top contact using other methods (e.g., chemical vapor deposition), leading ultimately to a controlled preparation of molecular electronic devices.

There have been previous investigations of ALD growth on SAMs of high-*k* materials[26,27] as well as metals (including copper).[28] In most of these studies (except for those unconcerned by interface damage[29]), copper was deposited on SAMs attached to (i) metallic substrates,[30−36] especially gold that conveniently reacts with thiol terminal groups, and (ii) oxide substrates (e.g., SiO_2/Si) using silanes molecules.[37,38] In all cases, probing the interface has been difficult due to limited sensitivity to interfacial chemical changes. For instance, X-ray photoelectron spectroscopy has limited sensitivity to buried interfaces and cannot easily determine if Cu penetrates the SAM grown on gold or on SiO_2 surfaces because of the nature of the interfaces. To avoid issues associated with the nature of the buried interface (e.g., SiO_2), SAMs should be attached to an oxide-free silicon substrate. Direct attachment of SAM is possible using molecules with an alkene end group, leading to the formation of a stable and well-defined Si−C interface, which is particularly attractive for microelectronic applications.[39] With this sample architecture (stacking sequence), the chemical modification of the Si/SAM interface, perturbation of the SAM layer itself, and metal interaction with the SAM headgroups can be monitored using IR absorption and X-ray photoelectron spectroscopies, for instance, without ambiguity due to substrate composition or stability.

This method to achieve the required level of perfection involves the preparation of carboxyl-terminated alkyl monolayers and the use of a newly synthesized copper precursor, copper di-*sec*-butylacetamidinate $[Cu(sBu\text{-}amd)]_2$. This precursor makes it possible to deposit metallic copper using molecular hydrogen at moderate temperatures (∼150 °C).[40,41] A common way to attach carboxyl-terminated alkyl monolayers on H-terminated silicon surfaces is based on a one-step hydrosylilation procedure using alkyl chains with alkene and carboxylic acid end groups.[42,43] Although this method yields good quality SAMs, on which metal oxides (e.g., Al_2O_3) have been successfully deposited by ALD,[26] the packing of these SAMs are not good enough to avoid some metal penetration and interface oxidation.[44] Therefore, a two-step procedure was used attaching first the molecules with an alkene and ester end groups and then transforming the ester termination into a carboxylic acid termination.[45,46]

Using this approach, we show that (i) carboxyl-terminated alkyl mololayers can be prepared with the same high density and quality as those achieved for less versatile methyl-terminated alkyl monolayers, characterized by electrical properties that are not dominated by interface defects; (ii) Cu is deposited with ALD, establishing an atomic contact with the SAM; (iii) a bidentate complexation occurs between the Cu and the COOH groups during the first half cycle of the ALD reaction; and (iv) the Si/SAM interface remains chemically intact after metal deposition.

(15) Fisher, G. L.; Walker, A. V.; Hooper, A. E.; Tighe, T. B.; Bahnck, K. B.; Skriba, H. T.; Reinard, M. D.; Haynie, B. C.; Opila, R. L.; Winograd, N.; Allara, D. L. *J. Am. Chem. Soc.* **2002**, *124*, 5528–5541.
(16) Hooper, A.; Fisher, G. L.; Konstadinidis, K.; Jung, D.; Nguyen, H.; Opila, R.; Collins, R. W.; Winograd, N.; Allara, D. L. *J. Am. Chem. Soc.* **1999**, *121*, 8052–8064.
(17) Chiechi, R. C.; Weiss, E. A.; Dickey, M. D.; Whitesides, G. M. *Angew. Chem., Int. Ed.* **2008**, *47*, 142–144.
(18) Holmlin, R. E.; Haag, R.; Chabinyc, M. L.; Ismagilov, R. F.; Cohen, A. E.; Terfort, A.; Rampi, M. A.; Whitesides, G. M. *J. Am. Chem. Soc.* **2001**, *123*, 5075–5085.
(19) Magnussen, O. M.; Ocko, B. M.; Deutsch, M.; Regan, M. J.; Pershan, P. S.; Abernathy, D.; Grubell, G.; Legrand, J. F. *Nature* **1996**, *384*, 250–252.
(20) Rampi, M. A.; Schueller, O. J. A.; Whitesides, G. M. *Appl. Phys. Lett.* **1998**, *72*, 1781–1783.
(21) Rampi, M. A.; Whitesides, G. M. *Chem. Phys.* **2002**, *281*, 373–391.
(22) Selzer, Y.; Salomon, A.; Cahen, D. *J. Am. Chem. Soc.* **2002**, *124*, 2886–2887.
(23) Selzer, Y.; Salomon, A.; Cahen, D. *J. Phys. Chem. B* **2002**, *106*, 10432–10439.
(24) Slowinski, K.; Fong, H. K. Y.; Majda, M. *J. Am. Chem. Soc.* **1999**, *121*, 7257–7261.
(25) Slowinski, K.; Majda, M. *J. Electroanal. Chem.* **2000**, *491*, 139–147.
(26) Li, M.; Dai, M.; Chabal, Y. J. *Langmuir* **2009**, *25*, 1911–1914.
(27) Preiner, M. J.; Melosh, N. A. *Langmuir* **2009**, *25*, 2585–2587.
(28) Fisher, G. L.; Hooper, A. E.; Opila, R. L.; Allara, D. L.; Winograd, N. *J. Phys. Chem. B* **2000**, *104*, 3267–3273.
(29) Xu, D.; Kang, E. T.; Neoh, K. G.; Zhang, Y.; Tay, A. A. O.; Ang, S. S.; Lo, M. C. Y.; Vaidyanathan, K. *J. Phys. Chem. B* **2002**, *106*, 12508–12516.
(30) Aldakov, D.; Bonnassieux, Y.; Geffroy, B.; Palacin, S. *ACS Appl. Mater. Interfaces* **2009**, *1*, 584–589.
(31) Baunach, T.; Kolb, D. M. *Anal. Bioanal. Chem.* **2002**, *373*, 743–748.
(32) Cavalleri, O.; Gilbert, S. E.; Kern, K. *Surf. Sci.* **1997**, *377−379*, 931–936.
(33) Czanderna, A. W.; King, D. E.; Spaulding, D. *J. Vac. Sci. Technol., A* **1991**, *9*, 2607–2613.
(34) Gilbert, S. E.; Cavalleri, O.; Kern, K. *J. Phys. Chem.* **1996**, *100*, 12123–12130.
(35) Whelan, C. M.; Ghijsen, J.; Pireaux, J. J.; Maex, K. *Thin Solid Films* **2004**, *464*, 388–392.
(36) Zangmeister, C. D.; Van Zee, R. D. *Langmuir* **2003**, *19*, 8065–8068.
(37) Bao, J.-Q.; Wang, Q.; Liu, X.; Ding, L. *Surf. Sci.* **2008**, *602*, 2250–2255.
(38) Liu, X.; Wang, Q.; Chen, L.-P. *Appl. Surf. Sci.* **2009**, *255*, 3789–3794.
(39) Cerofolini, G. F.; Romano, E. *Appl. Phys. A* **2008**, *91*, 181–210.
(40) Li, Z. W.; Rahtu, A.; Gordon, R. G. *J. Electrochem. Soc.* **2006**, *153*, C787–C794.
(41) Lim, B. S.; Rahtu, A.; Gordon, R. G. *Nat. Mater.* **2003**, *2*, 749–754.
(42) Boukherroub, R.; Wojtyk, J. T. C.; Wayner, D. D. M.; Lockwood, D. J. *J. Electrochem. Soc.* **2002**, *149*, H59–H63.
(43) Faucheux, A.; Gouget-Laemmel, A. C.; de Villeneuve, C. H.; Boukherroub, R.; Ozanam, F.; Allongue, P.; Chazalviel, J. N. *Langmuir* **2006**, *22*, 153–162.
(44) Seitz, O.; Li, M.; Dai, M.; Chabal, Y. J., paper in preparation.
(45) Boukherroub, R.; Wayner, D. D. M. *J. Am. Chem. Soc.* **1999**, *121*, 11513–11515.
(46) Liu, Y.-J.; Navasero, N. M.; Yu, H.-Z. *Langmuir* **2004**, *20*, 4039–4050.

2. Materials and Methods

2.1. General Information. Si(111) wafers (Fz, n-type, double side polished with a nominal resistivity of 1−20 Ω·cm) were purchased from Virginia Semiconductor. Nanopure deionized water (DIW) with a resistivity of 18.2 MΩ·cm and a total organic carbon (TOC) below 5 ppb was obtained from a Millipore system. Ethyl acetate (HPLC grade), acetone (ACS grade), dichloromethane (HPLC grade), hydrogen peroxide 30% (ACS grade), dimethylsulfoxide (DMSO, ACS grade), hydrochloric acid, and sulfuric acid (ACS plus grade) were all from Fisher and used as received. Potassium *tert*-butoxide 95% (Sigma-Aldricht), hydrofluoric acid 49% (CMOS grade, J.T. Baker), and ammonium fluoride 40% (CMOS grade, J.T. Baker) were also used as received. Ethyl undecylenate 97% (Aldricht) and 1-octadecene 95% (Fluka) were dried before reactions, respectively with molecular sieves and metallic sodium, and kept in a nitrogen environment. The copper precursor, copper di-*sec*-butylacetamidinate $[Cu(sBu\text{-}amd)]_2$, is commercially available through Rohm and Haas and has extensively been studied by Gordon et al.[40,41]

2.2. General Sequence of Events. A brief description of the sequence of events is described in this paragraph. Details of each step are described in the following paragraphs. (a) Cleaning of the silicon surface with its native oxide. (b) Hydrogenation of the surface. (c) Adsorption of the SAM with the ester end groups. (d) Transformation from the ester to the carboxyl end groups. (e) Introduction into the ALD reactor. (f) Annealing of the sample for stability test. (g) First $^1/_2$ of ALD cycle of Cu deposition. (h) First $^1/_2$ of ALD cycle of H_2 dosing. Additional 19 full ALD cycles. (i) Sample taken out of the chamber for further characterization.

2.3. SAMs Preparation. Wafers are cut into rectangular samples 3.8 cm by 6.8 cm and were cleaned by sequential rinsing in a flowing stream of DIW, ethyl acetate, acetone, and DIW. This step is mainly used to eliminate grease from the manipulation of the samples and the particles due to the sample cut. Subsequently, the samples were immersed in piranha solution (98% H_2SO_4/30% H_2O_2, 3:1, v/v) at 90 °C for at least 30 min and rinsed with copious amounts of DIW. The purpose of this step is mainly to have a perfectly clean surface for the SiO_2 reference measurement in Fourier transform infrared (FTIR) spectroscopy. The Si−H surface is then prepared by 1 min etching in diluted hydrofluoric acid (1:2, v/v with DIW) followed by 2 min 30 s in ammonium fluoride. The sample is then briefly rinsed with DIW and ready for SAM adsorption. Before reaction to form the SAM, the FTIR spectrum is recorded at this step for Si−H reference. Alkyl monolayers were formed via thermal hydrosilylation of alkenes. The freshly etched Si sample is immersed in neat deoxygenated octadecene or ethyl undecylenate under argon and heated at 200 °C for 4 h. After the reaction, the derivatized silicon sample is removed, rinsed with ethyl acetate (by sonication for 3 min), then further cleaned by immersion in boiling dichloromethane, and dried under a stream of nitrogen gas. The activation of the ester terminated surface (−COOEth) to the carboxylic acid terminated surface (−COOH) is done via subsequent immersion for 1 min 30 s in 0.25 M potassium *tert*-butoxide in DMSO, 30 s in pure DMSO, 30 s in HCl 2 M, and 30 s in DIW.

2.4. ALD Process. After activation of the COOH-terminated SAM, the sample is introduced into a home-built ALD reactor connected to an *in situ* FTIR spectrometer. The Si(111)-(CH_2)10-COOH sample is preannealed for 5 min at 185 °C in dry N_2 gas (300 sccm flow), purified in a Centorr model 2A N_2 purifier ($<10^{-8}$ Torr H_2O and O_2 pressures), to test the stability of the SAMs and remove physically adsorbed water. During ALD processing, the system is continuously pumped at all times. A column bubbler containing the copper precursor $[Cu(sBu\text{-}amd)]_2$ is kept at 90 °C. The ALD is done at a substrate temperature of 185 °C. The effective exposure time to the copper precursor is 35 s, equivalent in our chamber to 185×10^6 langmuir (L), and the effective exposure to H_2 is 300 s, equivalent to 21×10^{10} L. However, because of the purging time in between the exposures (∼500 s), the time for a full ALD cycle ($[Cu(sBu\text{-}amd)]_2 + H_2$) is ∼21 min. For most experiments, 20 ALD cycles are used leading to a sample soaked at 185 °C for at least 7 h (if no IR measurements are taken in between cycles) and an upper limit of 15 h at a temperature ranging from 60 to 185 °C (if IR measurements are taken).

2.5. FTIR *in Situ* and *ex Situ*. *In situ* IR absorption measurements (4 cm^{-1} resolution) are performed in transmission (∼70° incidence) through two KBr IR windows with a Nicolet Nexus 670 equipped with an external MCT-B detector. These KBr windows are protected from moisture and contamination during ($[Cu(sBu\text{-}amd)]_2$ and H_2 exposure by closing two gate valves separating the windows from the reactor during precursor exposure. To maintain good temperature control and minimize the artifacts due to bulk silicon phonon absorption, the sample temperature is kept at 60 °C for data acquisition and raised to 185 °C during ALD growth. During acquisition, the chamber is constantly purged with flowing nitrogen (∼50 sccm). To investigate the interaction between the COOH-terminated SAM and the precursor, FTIR spectra are recorded in between each exposure for the first two half cycles.

Ex situ IR absorption measurements (4 cm^{-1} resolution) are performed in transmission (∼70° incidence) with a Nicolet Nexus 6700 with an internal DTGS detector. As the spectrometer is installed in an ultrahigh purity glovebox (O_2 and $H_2O < 0.1$ ppm), no degradation of the surface occurs while the reference Si−H sample is measured and introduced into the reaction solution.

All absorption spectra are calculated using at least three averaged spectra of 500 scans of the modified and the reference sample.

2.6. Current−Voltage (*I*−*V*) Measurements. *I*−*V* measurements of the molecules are performed using *n*-Si/molecules/Hg junctions. The junctions are formed by placing a Hg (99.9999% purity) drop on the SAM, using a controlled growth hanging mercury drop (HMD) electrode apparatus (BAS, U.S.A.). The Si samples are contacted on the back by applying In−Ga eutectic, after scratching the back surface with a diamond-edge knife. The contact area between the Hg drop and the monolayer is in the range of 0.5 mm in diameter. The *I*−*V* characteristics are collected using an HP 4155 semiconductor parameter analyzer in voltage scan mode. Several scans, in the range from −1 to 1 to −1 V, are measured for each junction with a scan rate of 20 mV/s. At least 10 junctions are made on each sample, and the results represent the average of all the measurements.

2.7. XPS Characterization. The high resolution XPS data are obtained using an Omicron Nanotechnology system equipped with an Al Kα monochromatic X-ray source (0.25 eV line width) and a hemispherical analyzer (pass energy = 15 eV) with a lens acceptance angle of 16° and seven Channeltron detectors, described elsewhere.[47] The sample surface is tilted at 45° with respect to the analyzer detector. The nominal pressure in the analysis chamber is better than 2×10^{-10} mbar.

2.8. AFM Characterization. The AFM images are recorded with a Veeco Digital Instrument Nanoscope Dimension 3100 in ambient atmosphere. The tool is disposed on a free-vibration table and enclosed inside a free-acoustic cover during the measurement. All the measurements are done in tapping mode with a resolution of 512 points per line. For SAM covered substrates, the acquisition was performed at 3.05 Hz (less sensitive to noise for very flat surfaces), while after Cu deposition, due to the large increase of roughness, the acquisition is done at 0.75 Hz.

3. Results

3.1. Characteristics of SAM Layers. 3.1.1. Vibrational Measurements. The method developed to attach COOH-terminated SAMs on oxide-free Si surfaces involves the immersion of H-terminated Si surfaces in ethyl undecylenate (first processing step), followed by −COOEth to −COOH transformation

(47) Wallace, R. M. *ECS Transactions* **2008**, *16*, 255–271.

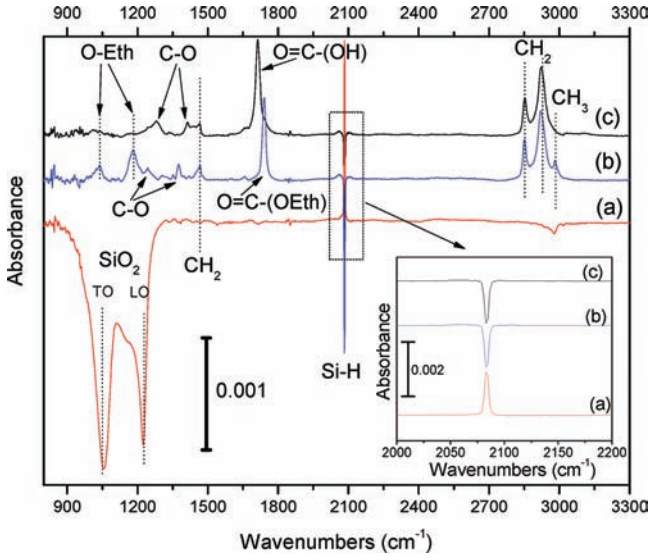

Figure 1. Absorption spectra of (a) hydrogenated Si (111) surface, (b) COOEth terminated SAM, and (c) COOH terminated SAM. (a) is referenced to the surface with it cleaned native oxide; (b) and (c) are referenced to the Si−H surface. No SiO_2 is observed after all of the SAM preparation process. Inset: Zoom on the Si−H vibration modes on the different surfaces.

(second processing step) as described in the method. Figure 1 shows the spectra at three critical stages: (1) a fully H-terminated surface (Figure 1a), characterized by a strong Si−H stretch mode at 2083 cm^{-1} (integrated intensity = 0.0084 cm^{-1}); the spectrum also displays at low frequencies two negative bands at 1224 and 1055 cm^{-1}, corresponding to the loss of the SiO_2 longitudinal (LO) and transversal optical (TO) phonon modes (respectively) of the reference surface; (at higher frequencies ~2920 cm^{-1}, the negative feature originates from the removal of hydrocarbon contaminants adsorbed on the hydrophilic SiO_2 reference surface during exposure to ambient atmosphere); (2) a surface terminated by a COOEth-terminated alkyl chain (Figure 1b) obtained after the first processing step; and (3) a surface terminated by COOH after the second processing step (Figure 1c). The inset in Figure 1 shows that a substantial amount of the initial Si−H stretch mode is lost after molecular adsorption.[48] Based on the integrated area of Si−H remaining on the surface (Figure S1 in the Supporting Information), 35% ± 5% of the initial hydrogen atoms are still on the surface at the end of the two step process.

Importantly, there is no evidence in spectra b and c for any oxide formation. Indeed, after removal of the SAM spectral features from these two spectra, an upper limit for SiO_2 formation (see Supporting Information) of 4% of a monolayer can be established based on the baseline accuracy (signal-to-noise) in the 900−1300 cm^{-1} region.

The degree of chemical modification of the COOEth terminated SAM to form a COOH terminated SAM can be examined by comparing spectra b and c. Before chemical reaction (Figure 1b), two features present at 1037 and 1180 cm^{-1}, assigned to the O−Eth bending and stretching vibrations respectively, are absent in spectrum (c), suggesting that the $-CH_2-CH_3$ group is removed. Moreover, the two peaks at 1242 and 1375 cm^{-1}, assigned to the bending and stretching modes of the C−O of the COOEth entity respectively, are shifted to 1280 and 1412 cm^{-1} for the COOH-terminated surface. These shifts are consistent with the different environment of the C−O vibration in its two configurations (C−OEth vs C−OH). Moreover, the strong mode that appears at 1741 cm^{-1} on the COOEth-terminated surface, assigned to the stretching mode of the carbonyl group (C═O), is shifted to 1712 cm^{-1} for the COOH-terminated surface, due to two different environments. These frequencies agree with values previously reported for the two different systems[45,46] and confirm the complete chemical transformation of the SAM headgroups. Finally, the characteristic CH_3 mode at 2981 cm^{-1} of the COOEth-terminated surface is absent on the COOH-terminated surface, further confirming the successful headgroup transformation.

The ultimate assessment of the SAM quality comes from the degree of packing density. A sensitive measure of the SAM packing is the values of the asymmetric CH_2 stretch modes.[49−51] For highly packed films, a stronger interaction among neighboring alkyl chains leads to a lower stretch frequency. For this system (Figure 1c), the mode appears at 2921 cm^{-1}, which is lower than that achieved by the traditional one-step process[26] yielding 2926 cm^{-1}. This value is essentially the same as that observed for the COOeth-terminated surface, namely 2920 cm^{-1} in spectrum (b), indicating that little perturbation of the alkyl chain occurs upon chemical modification of the headgroups. Another measure of the packing density is the frequency of the C═O vibration that is red-shifted when the chains are more packed due to H bonding of the neighboring C═O moieties. In spectrum (c), the C═O vibration is at 1712 cm^{-1}, which is consistent with highly packed surfaces.[52]

3.1.2. Electrical Measurements. Electrical properties are a sensitive measure of the SAM quality. Using a Hg electrode top contact, the conductivity of the COOEth-terminated surface is studied and compared to a well-known CH_3-terminated SAM (containing 18 carbons) reference system. Figure 2 shows the $I-V$ measurements obtained for n-Si-$C_{17}H_{34}-CH_3$//Hg junctions that are (a) with and (b) without oxide contamination,[53] respectively, and for an n-$SiC_{10}H_{20}$-COOEth//Hg junction (Figure 2c). For the two surfaces that are of high electrical quality, curves (c) and (b), the $I-V$ curves are coincident at low forward bias (from 0 to +0.3 V). Above 0.3 V, the curves split when the tunneling regime starts to dominate the transport (i.e., depends on chain length). As discussed in more detail later, the degree of coincidence makes it possible to assess the quality of the monolayer. In comparison, a nonideal junction (containing an oxide contamination as shown in Figure 2a) shows obvious differences. Much more current can flow through the junction ((a) vs (c)) because of the lower (Schottky) barrier, at low bias (4.2×10^{-6} A vs 2.8×10^{-9} A at +0.2 V respectively). At

(48) As SAMs react with the H-terminated surface, the dipole coupling between the remaining Si−H is weakened, resulting in a broadening and a red shift of the Si−H stretch modes. Consequently, the *differential* spectra in Figure 1b and 1c show a sharp negative component next to a broader and weaker positive absorption on the lower frequency side. The amount of H removed is ~65% as discussed in the Supporting Information using Figure S1 in which an oxidized surface is used as reference.

(49) Snyder, R. G.; Strauss, H. L.; Elliger, C. A. *J. Phys. Chem.* **1982**, *86*, 5145–5150.
(50) Porter, M. D.; Bright, T. B.; Allara, D. L.; Chidsey, C. E. D. *J. Am. Chem. Soc.* **1987**, *109*, 3559–3568.
(51) Aswal, D. K.; Lenfant, S.; Guerin, D.; Yakhmi, J. V.; Vuillaume, D. *Anal. Chim. Acta* **2006**, *568*, 84–108.
(52) Gershevitz, O.; Sukenik, C. N. *J. Am. Chem. Soc.* **2004**, *126*, 482–483.
(53) Interfacial oxide is considered in the system as a contamination since it is an unwanted species. This oxide is the standard native oxide that would grow if the surface of silicon was not protected by the SAM. The presence of an oxide reflects the imperfection of the SAM and is considered a contamination.

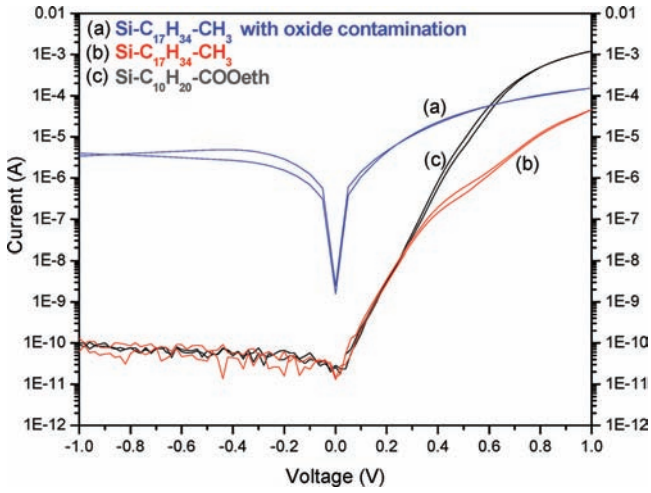

Figure 2. Current−voltage curves for *n*-Si-$C_{17}H_{34}$−CH_3//Hg junctions that are (a) with and (b) without oxide contamination. (c) Current−voltage curve for *n*-$SiC_{10}H_{20}$-COOEth//Hg junction. The COOEth terminated SAM has a sufficient quality so that the *I*−*V* measurements reflect the presence of the molecules (i.e., not dominated by the defects).

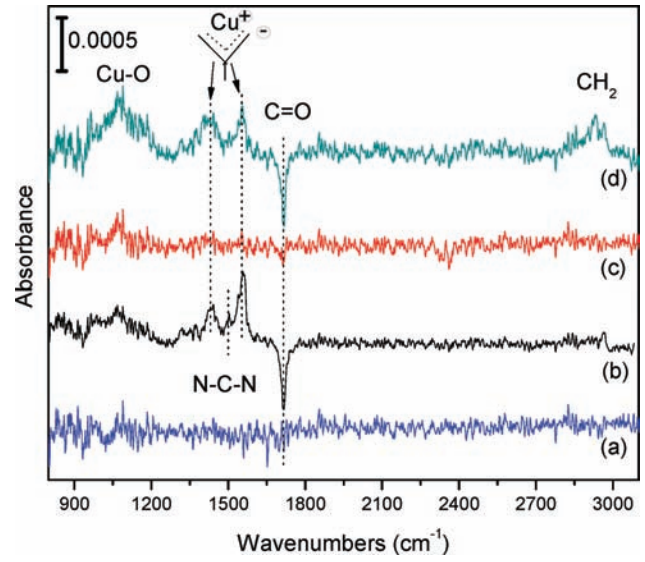

Figure 3. Absorption spectra of (a) COOH-terminated SAM annealed at 185 °C for 5 min, (b) after first half cycle of ALD Cu deposition, (c) after first half cycle of H_2 flow, and (d) after the full 20 ALD cycles. (a) is referenced to the freshly prepared COOH-terminated SAM; (b), (c), and (d) are referenced to the COOH-terminated SAM annealed at 185 °C for 5 min.

higher bias, the tunneling current of defective SAMs (Figure 2a) is higher (1.5×10^{-4} A at 1 V) than that of higher quality SAMs (4.5×10^{-5} A at 1 V) (Figure 2b).

3.2. ALD Deposition of Cu. To investigate the Cu deposition on such SAMs, the fresh COOH-terminated SAM is loaded into the ALD chamber immediately. Before initiating the ALD process, the stability of the SAM layer is examined by annealing the sample at 185 °C for 5 min. Figure 3a shows the absorption spectrum of the SAM after annealing, referenced to the spectrum of the initial SAM, both taken at 60 °C. No observed absorption or changes in absorption over the whole spectral range confirms that the SAM remains stable (below our ability to measure SiO_2, namely ∼20% SiO_2 monolayer; see Supporting Information). These SAMs can therefore withstand the thermal budget (∼185 °C) necessary for the ALD process, and changes observed during this process are therefore not due to the degradation of the SAM.[54] In fact, our own FTIR studies on these SAMs (not shown here), confirmed by the literature results, have shown that these SAMs are extremely stable even at 200 °C for several hours.[55] Chemical changes such as loss and configuration modification (reaction in between the groups) of the COOH groups as well as distortion in the chains begin to be detected at 250 °C. At 300 °C, loss of the alkene chains becomes detectable.

Figure 3 shows the absorption spectra of the COOH-terminated surface after (b) the first $^1/_2$ cycle (precursor dosing) of the ALD copper deposition, (c) the second $^1/_2$ cycle (H_2 dosing), and (d) 20 full cycles. All these spectra are referenced to spectrum (a) recorded after annealing. After the first $^1/_2$ cycle, a variation in the C═O stretching mode is apparent: there is a negative peak at 1714 cm^{-1}, indicating that the Cu precursor chemically interacts with the SAM surface. There are also two positive bands appearing at 1562 and 1440 cm^{-1} (spectrum b), which have been assigned to the asymmetric and symmetric stretching modes of the C═O in acid salt structures (CO_2^-).[56] There is some contribution at 1500 cm^{-1}, characteristic of the N−C−N vibration of the ligand when linked to Cu. In the low frequency region, there is a broad and weak contribution centered at 1100 cm^{-1}, which is assigned to CuO. After H_2 dosing (Figure 3c), this CuO absorption is the only feature that remains, except for a very weak spectral loss at 1717 cm^{-1} (see Supporting Information Figure S2 for an expanded view of Figure 3c). In interpreting the spectrum, it is important to realize that pure Cu cannot be detected with IR spectroscopy until a more continuous film is formed because the Cu phonon frequencies are outside the range of the detector.

After 20 ALD cycles, the absorption spectrum (Figure 3d) shows a stronger absorption at ∼1000 cm^{-1}, indicating that there is a larger amount of CuO on the surface. Also, a strong negative feature at 1714 cm^{-1} and two positive bands at 1562 and 1440 cm^{-1} suggest that a large fraction of COOH groups have reacted. In the 2900 cm^{-1} region, the presence of additional CH_2 on the surface is detected and shows that even if the reaction induced by H_2 dosing is successful, not all of the ligands have left the surface.

Figure 4 summarizes the spectra obtained (a) before and (b and c) after the *in situ* growth process (20 cycles). These spectra are taken *ex situ* and referenced to a variety of starting surfaces to distinguish all relevant spectral features. Spectra (a) and (b) are referenced to the starting surface with the native oxide, which makes it possible to study the Si−H stretch region accurately and determine how much hydrogen is left after all the treatments. Spectrum (c) is referenced to the Si−H surface, which makes it possible to analyze in more detail the low frequency region (900−1300 cm^{-1}), without interference by the negative phonon bands due to the removal of the SiO_2 prior to SAM deposition. After 20 cycles, there is a fraction (integrated area of 0.004 cm^{-1}) of the original band (0.022 cm^{-1}) at 1712 cm^{-1} that remains. A CuO absorption band at ∼1100 cm^{-1} (spectrum c) is also observed. Of course, the asymmetric and symmetric

(54) The stability of the SAM was routinely checked for 5 min before any ALD deposition because we had noticed that good quality SAMs remain stable for long times (>15 h) and that poor quality SAMs degrade (with SiO_2 formation) in less than 5 min. Therefore, a 5 min check represents a convenient and fair method to assess quality.

(55) Faucheux, A.; Yang, F.; Allongue, P.; de Villeneuve, C. H.; Ozanam, F.; Chazalviel, J. N. *Appl. Phys. Lett.* **2006**, *88*, 193123–3.

(56) Socrates, G. *Infrared and Raman Characteristic Group Frequencies: Tables and Charts*, 3rd ed.; John Wiley & Sons, LTD: Chichester, West Sussex, 2004; p 128.

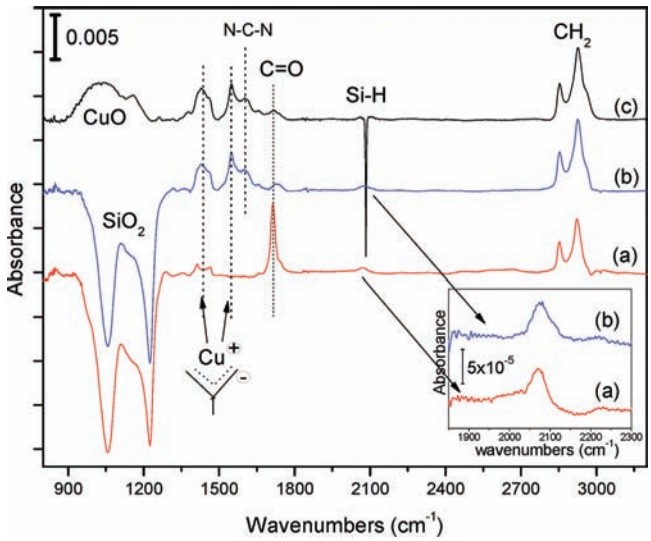

Figure 4. Absorption spectra of (a) COOH-terminated SAM and (b and c) COOH-terminated SAM with 20 Cu ALD cycles. (a) and (b) are referenced to the surfaces with the native oxide; (c) is referenced to the Si−H surface. Figure inset: zoom on the Si−H region before and after the 20 Cu ALD cycles. The amount of hydrogen at the interface after the ALD cycles is equivalent to the one before ALD treatment.

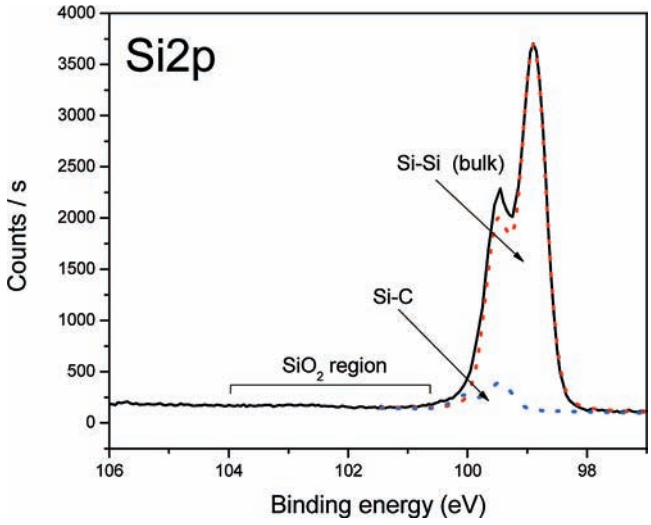

Figure 5. XPS spectrum of Si2p region of COOH-terminated SAM after 20 Cu ALD cycles. No SiO_2 is formed during and after the copper deposition.

stretching modes of the C═O in the acid salt structure (CO_2^-) are also observed. A new band appears at 1600 cm^{-1}. This band is assigned to the N−C−N stretch of the ligands that are *not* linked to the Cu, in contrast to the bonding configuration of the undissociated precursor.

3.3. *Ex Situ* Characterization of Si/SAM/Cu Stack by XPS. To confirm the FTIR results and obtain more information on the deposited copper, XPS measurements were performed on COOH-terminated SAMs after 20 ALD cycles. The XPS is first used to determine the degree of oxidation of the samples. Figure 5 shows the Si2p region. This measured Si2p spectrum is deconvolved in two spin−orbit split doublets $Si2p_{3/2}$−$2p_{1/2}$ at 98.9 and 99.5 eV and 99.5 and 100.1 eV, which correspond to bulk silicon and to silicon bound to a carbon atom, respectively. There is no observable intensity between 101 and 104 eV despite the good sensitivity to silicon. Given signal-to-noise ratio, and using the SiC component as calibration, an upper

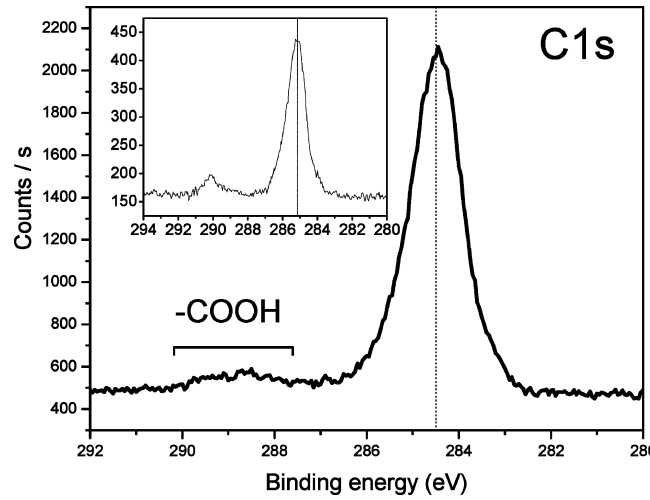

Figure 6. XPS spectra of C1s region of COOH-terminated SAM before (inset) and after 20 Cu ALD cycles. C with a COOH environment are still detectable. This is consistent with the FTIR results; viz. not all the groups on top of the SAM have reacted during the ALD process.

limit of 5.6% monolayer SiO_2 is obtained (see Supporting Information), which is consistent with the upper limit set by the more sensitive IR measurements (<4% ML calculated on the surface before Cu deposition).

The high resolution C1s XPS spectra before (inset) and after Cu deposition are shown in Figure 6. The main component centered at 284.6 eV is principally attributed to aliphatic hydrocarbons in the chains. The large intensity of these carbons makes it difficult to clearly identify the presence of C−Si at lower binding energies (~283 eV) and C−O at higher binding energies (~286 eV). However, a superposition of the two normalized spectra before and after copper deposition (see Supporting Information Figure S3) makes it possible to rule out any change in the C−Si and C−O components of the peak. On the other hand, there are variations observed at higher binding energies. The sharp O−C═O feature centered at 290 eV broadens and extends over a wider energy range (from 287.5 to 290 eV) after deposition, which is consistent with a change in the electronic environment of the acid group. The ratio of the integrated areas of the peaks corresponding to the aliphatic hydrocarbons and the acid group, (C═O/CH), changes from 0.079 before deposition to 0.065 after deposition, suggesting an increase of hydrocarbons on the surface.

As previously mentioned, the FTIR data are not sensitive to metallic Cu in low concentration, i.e. only CuO. XPS on the other hand can distinguish metallic Cu and CuO, as shown in Figure 7. We first focus on the high binding energy part of the Cu2p core level spectrum obtained on the COOH-terminated SAM after 20 ALD cycles. The deconvolution of this peak is done with two components centered at 932.0 and 933.1 eV, components that might have been better distinguished if a synchrotron source was used. The peak at 933.1 eV can unambiguously be attributed to copper with a Cu(+II) oxidation state, which confirms the presence of CuO on the surface. The presence of CuO may be due to (i) the interaction between the COOH and the Cu and/or (ii) the fact that these samples were transferred from the ALD reactor to the XPS chamber in ambient air with possible spurious oxidation. The peak at 932.0 eV is more difficult to assign. It may be due to metallic copper or cuprous oxide, Cu(0) or Cu(I) respectively. The binding energies are nearly identical, i.e. within the resolution of the XPS

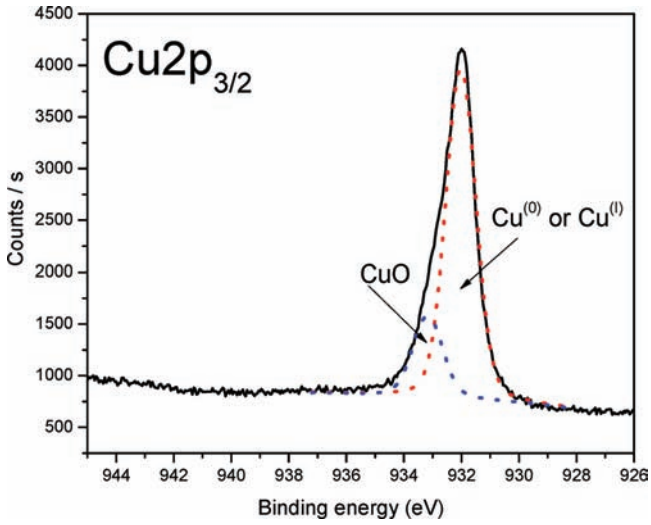

Figure 7. XPS spectrum of $Cu2p_{3/2}$ region of COOH-terminated SAM after 20 Cu ALD cycles. The deposited copper is mainly in the metallic state. Some of the copper is oxidized (CuO) due to the interface SAM-COOH// Cu and also due to the transfer done in ambient.

apparatus (±0.1 eV). An investigation of the Auger parameter utilizing the Cu LMM X-ray excited Auger feature and the Cu 932.0 eV peak indicates that the state is unambiguously Cu(0). Moreover, this is in excellent agreement with previous conductivity measurements of films deposited on SiO_2 surfaces using this copper precursor showing a conductivity consistent with metallic (Cu(0)) at least after hundreds of cycles.[40,41]

3.4. Cu Film Morphology. The above measurements indicate that Cu can successfully be deposited without damaging the SAM. However, it is also important to determine if the copper is homogeneously deposited on the surface. To that end, AFM topographic images have been carried out before and after Cu deposition and are shown in Figure 8. Figure 8a shows the AFM image of COOEth-terminated SAM before treatment. Because of the presence of the SAM, the step morphology of the hydrogenated Si surface is maintained and extremely stable.

After activation to the COOH-terminated surface and 20 Cu ALD cycles, grains of copper can clearly be seen in the 500 × 500 nm image, Figure 8b. Figure 8b indicates that the SAM surface is covered by smaller (<5 nm) grains that are closely packed, consistent with the observed modification of the SAM headgroup IR spectrum (∼80% coverage). Larger scale agglomeration appears to take place above this tightly packed layer, as evidenced by the presence of larger grains (∼10−50 nm) more loosely packed. On a larger scale (Figure 8c), the deposited copper is observed to be well spread over the whole surface, even if the overall image gives an impression of empty spaces within the grains because of the higher contrast from the last layer of copper grains.

4. Discussion

4.1. SAM Quality and Stability. As shown in the previous section, the quality of the SAM can be assessed from results of IR absorption, XPS, AFM, and electrical measurements. The absence of SiO_2 features in the IR spectra for both COOEth- and COOH-terminated SAMs is well corroborated by Si2p XPS data. IR and XPS results set an upper limit of 4% ML and 5.6% ML respectively. Namely, there is no deterioration of the Si−SAM interface when the headgroup transformation from COOEth to COOH is performed. The CH_3 stretching groups of the ethyl groups at 2981 cm^{-1} are completely removed, and there is a characteristic shift in the frequency of the C═O stretching vibration from 1741 cm^{-1} of COOEth to 1712 cm^{-1} of the COOH, which is in good agreement with the reported values for these systems.[45,46] The observed frequency of C═O on the COOH terminated SAM implies that there is hydrogen bonding between two neighboring units, forming O═C−OH---- O═C−OH. Indeed, the C═O frequency is known to red shift toward 1710 cm^{-1} when hydrogen bonding occurs between the groups,[52] which suggests high packing of the chains. The degree of packing is also correlated to the frequency of the CH_2 asymmetric stretching mode of the alkyl chains. These data show that, despite the presence of bulky headgroups, the alkyl chains are characterized by CH_2 frequencies (2920 and 2921 cm^{-1}) that are similar to the ones reported for high quality methyl-terminated alkyl chains with an equivalent number of carbons (C12, 2920 cm^{-1}). This result indicates that good packing is possible even with large headgroups. For COOEth and COOH-terminated[57]SAMs, the Si−H integrated area (0.0029 cm^{-1} and 0.0026 cm^{-1}, respectively) remaining on the surface represents ∼30% and ∼35% of the initial H coverage (0.0084 cm^{-1}), indicating that 65% ± 5% of the sites have reacted with the C═C alkene groups. This value is somewhat higher than what has been reported/calculated in the literature (∼50%)[43,58] but clearly indicates that the packing density is high. AFM topographic images provide a more visual way to attest to the high density and stability of the SAMs. Indeed, the underlying step structure of the substrate can be seen after full homogeneous coverage of the surface by the SAM. The high SAM density protects the interface from oxidation for period of weeks, as verified by IR spectroscopy.

A method to characterize the interface integrity that is more sensitive than all the previously mentioned techniques (FTIR, AFM, and XPS) is based on electrical measurements. Indeed, the current flowing in the junction (from the substrate to a top contact) is sensitively dependent on a low concentration of defects, although it cannot distinguish the type of defects. This approach, using mercury as a top electrode, has been used previously to ascertain that electrical transport through a molecular film is not dominated by defects in the molecules and/or the film.[57]

A good agreement was shown to occur over the complete forward bias range between measured current−voltage curves for a series of *n*-Si/C_nH_{2n+1}/Hg junctions (n = 12, 14, 16, and 18) and a theoretical model for a metal/ideal insulator/semiconductor structure.[59] This model treats thermionic emission (TE) over the Schottky barrier in the semiconductor and tunneling through the insulating barrier as two coupled processes. *Because no defects are included in the theoretical model,*[60] the agreement lends credence to the notion that, for very high-quality SAMs, the properties of the molecules rather than those of defects in the SAM dominate the transport characteristics. Differences between SAM qualities are clearest in the TE rather than in the tunneling region.

In the present work, an identical interface is expected between the *n*-Si/C_nH_{2n+1}/Hg junctions and the *n*-Si/$C_{10}H_{20}$-COOEth/Hg

(57) Seitz, O.; Bocking, T.; Salomon, A.; Gooding, J. J.; Cahen, D. *Langmuir* **2006**, *22*, 6915–6922.
(58) Sieval, A. B.; van den Hout, B.; Zuilhof, H.; Sudholter, E. J. R. *Langmuir* **2001**, *17*, 2172–2181.
(59) Salomon, A.; Boecking, T.; Chan, C. K.; Amy, F.; Girshevitz, O.; Cahen, D.; Kahn, A. *Phys. Rev. Lett.* **2005**, *95*, 1–4.
(60) Shewchun, J.; Dubow, J.; Myszkowski, A.; Singh, R. *J. Appl. Phys.* **1978**, *49*, 855–864.

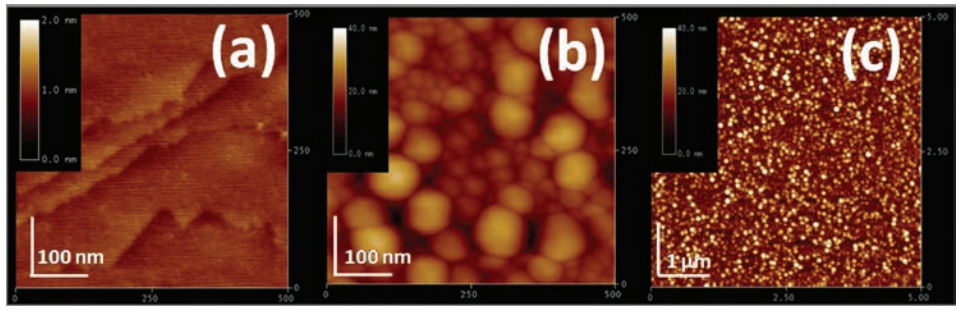

Figure 8. AFM pictures of COOEth-terminated SAM (a) before and (b and c) after activation of the surface to the COOH-terminated surface and 20 Cu ALD cycles. (a) and (b) are 500 × 500 nm^2 images; (c) is a 5 × 5 μm^2 image. Before ALD, the silicon surface is stabilized by the presence of the SAM, a good indication of the high quality of the SAM. After ALD, the Cu is in a granular form and well spread on the surface.

junctions. Therefore, the same behavior is expected in the TE regime with only a difference in the tunneling region due to the chain length. This behavior is observed precisely in our measurements, where both curves are superposed at low forward bias and split in two when the tunneling regime starts to dominate the transport. The $I-V$ measurement strongly confirms the high quality of the SAMs preparation and their potential to be used for devices. Furthermore, these COOH-terminated SAMs are easier to prepare than thiol-terminated SAMs of equivalent qualities and more versatile than methyl-terminated alkyl monolayers.

4.2. Copper Deposition. With well-characterized SAMs, it is now possible to investigate in detail the copper layer as well as the Si/SAM and COOH/Cu interfaces.

4.2.1. The Copper Layer. IR spectroscopy provides most of the mechanistic information on the growth since it is performed *in situ*. *Ex situ* AFM and XPS are then useful to confirm the conclusions drawn from IR spectroscopy. Spectrum (a) in Figure 3 confirmed that the SAM remains stable at 185 °C, which is the required temperature for ALD growth, so that any spectral change can be attributed to the ALD process and not to the SAM degradation.

After the first $^1/_2$ Cu cycle exposition, the Cu precursor clearly interacts with the carboxyl group and forms an acid salt structure. This conclusion is seen in spectrum (b) of Figure 3 by the intensity loss at 1714 cm^{-1} and the detection of the two bands corresponding to the asymmetric and symmetric stretching modes of the C═O in the acid salt structure. The presence of intact ligands that are still linked to the Cu is also evident in spectrum (b) of Figure 3. After the first $^1/_2$ H_2 cycle, these ligand modes are not present any longer, which indicates that the expected ALD reaction has taken place. However, while H_2 releases these ligands from the precursor molecules, the intensity loss at 1714 cm^{-1} is less than that before H_2 exposure; namely the number of reacted COOH groups has decreased. This indicates that the initial surface characterized by "free" COOH groups is partly recovered. This observation suggests that the free copper ions on the surface agglomerate into clusters, leading to the reformation of COOH groups on top of the SAM. This agglomeration leading to an inhomogeneous surface is confirmed by topographic AFM images after Cu deposition (Figure 8b). In fact, copper is known to agglomerate and form grains on most surfaces, such as oxide surfaces.[41,61] In this case, the acid salt interaction between Cu and the SAM headgroups appears to also be reasonably weak, since the agglomeration is not hindered. Consequently, Cu does agglomerate to form nanoparticles, characterized by a size distribution ranging from 40 to 80 nm after only 20 cycles (Figure 8b).

During the two first $^1/_2$ cycles, CuO formation can also be detected in the low frequency region (∼1000−1200 cm^{-1}). After 20 cycles, the CuO phonon mode is clearly identified, in both *in situ* and *ex situ* IR measurements, by a strong band centered at ∼1100 cm^{-1}. The presence of cupric oxide is also confirmed by XPS measurements (Figure 7). The XPS data also show that there is metallic Cu, a fact that could not be derived from FTIR measurements (Cu−Cu modes outside the range of detection). The area analysis of the Cu2p$_{3/2}$ components (Cu and CuO) shows that 23% of the detected copper is in an (+II) oxidized form (CuO). This amount of CuO is definitely overestimated because of the additional oxide that forms during the transfers in air from the ALD chamber to the XPS chamber. A comparison of the integrated area of the C═O stretching mode before (0.022 cm^{-1}) and after (0.004 cm^{-1}) ALD cycles shows that more than 80% of the COOH groups have reacted by the end of the ALD process. Furthermore, the blue shift of the C═O stretching before and after Cu deposition (from 1712 cm^{-1} to 1725 cm^{-1}) indicates that the COOH groups are not interacting (i.e., they are characterized by isolated frequencies). These two observations suggest that there is almost a complete spreading of Cu on the surface, despite the formation of Cu clusters.

The IR spectra make it possible to determine the purity of the Cu layer. The presence of ligands remaining at the surface, even after the H_2 pulses, is evident by the observation of the mode at 1600 cm^{-1}. These ligands are not bonded to Cu and therefore constitute an impurity trapped at the surface on or in the Cu layer. The presence of extra carbon is also evident in the XPS spectra (Figure 6) with a 20% increase after Cu deposition. After 20 cycles, there is an ∼1 nm thick Cu layer on average as determined by RBS measurements (see Supporting Infomation Figure S4), consistent with previous work by Gordon et al.[41] The morphology is highly inhomogeneous, resulting in the presence of very thin (≪1 nm) areas on the surface and clusters. As a result, the underlying Si substrate is still easily detectable by XPS (Figure 5).

4.2.2. The Si/SAM Interface. There are two ways to determine the chemical quality of the Si/SAM interface, i.e. to quantify how much SiO_2 or other interfacial contamination may exist at the interface after the Cu ALD process, based on IR and XPS data.

One way is to detect and quantify the presence of SiO_2 at the interface. It is difficult to extract sensitive information from the IR absorption data shown in Figure 4c because there is absorption from CuO in the same spectral region. Therefore, we use the complementary HR-XPS measurements of the Si2p

(61) Dai, M.; Kwon, J.; Halls, M.; Gordon, R. G.; Chabal, Y. J., submitted.

region after Cu deposition. These spectra show no feature between 101 and 104 eV within our detection limit (i.e., < 5.6% ML). This observation confirms that the interface remains unoxidized, oxidation that would have definitely taken place while the sample is transferred in air from the ALD chamber to the XPS chambers if the SAM had been damaged.

A second way to probe this interface is by focusing on specific interfacial species, namely the Si−H left on the surface after formation of the SAM. If the Si−H are protected by the SAM (against Cu diffusion, for instance), no changes should occur after deposition. To check this hypothesis, the integrated areas of the Si−H stretch mode are compared before and after Cu deposition (Figure 4 inset). These areas are identical within the error bar (5%) due to the baseline positioning. This is a significant observation that is only possible for the type of substrate/SAM system here. Indeed, it is not possible to determine the integrity of the substrate/SAM interface in systems used previously, such as metal or SiO_2 substrates. In this present study of Si/Cu, we can conclude that the SAM efficiently prevents Cu diffusion. Such information could not have been as clearly obtained with standard XPS measurements.

4.2.3. The COOH/Cu Interface. The main observation for this interface, gathered from IR absorption and XPS data, is that the Cu precursor reacts with the carboxylic group. This chemical reaction, expected for a proper ALD process, is observed in the disappearance of the C═O bond as shown in Figure 3b and 3d (IR absorption) and Figure 6 (XPS). As a result, the functionalized surface is atomically smooth and uniform as seen with AFM (Figure 8b and c). An analysis of the FTIR spectra reveals that 80% of the COOH groups have reacted. From the C1*s* core level in XPS, it is clear that most, if not all, of the HO−C═O groups are still present but in a different electronic configuration (broader C1*s* contribution at 289 eV shown in Figure 6 compared to ∼290 eV region in inset). To quantify these features, the ratios of the integrated areas of the peaks corresponding to the acid group (∼289 eV) and the aliphatic hydrocarbons (∼284.5 eV) are examined before and after Cu deposition. There is only a minor decrease from 0.08 to 0.065 in these ratios, due to an increase of aliphatic hydrocarbons. This increase indicates that some ligands from the Cu precursor are trapped inside or on top of the Cu layer, consistent with the IR absorption observation (Figure 3d). The conclusion that no COO group is lost is in good agreement with the reported results of Whelan et al.[35] These groups remain present, but in a different environment, namely with formation of a COO^- acid salt structure, consistent with the strongly shifted CO modes of this salt structure (Figure 3d).

There are two possible bonding configurations for Cu on COOH: (i) the unidentate Cu bond resulting from a reaction either with hydroxyl or with the carbonyl group and (ii) the bidentate Cu bond involving both the OH and C═O groups. Czanderna et al.[33] rejected the possibility of having a chemical interaction of the C═O bond with copper, and Whelan et al.[35] concluded that the copper interact most likely via a unidentate complexation through the hydroxyl group. In contrast, the IR absorption data clearly show that a complexation through carboxylic groups and also with the hydroxyl groups takes place, leading to a bidentate configuration. This configuration is confirmed by the observation of the asymmetric and symmetric stretching modes of O−C═O in acid salt structure (CO_2^-) associated with the loss of C═O mode of the carboxylic acid group.

The observation of a predominant bidentate structure is therefore associated with Cu deposition using ALD, involving the interaction of a Cu precursor with COOH. The deposition methods used by Czanderna et al.[33] and Whelan et al.[35] are based on metal evaporation. It is therefore conceivable that such methods lead to a different bonding configuration because elemental Cu can react directly with the hydroxyl or carbonyl groups. Since evaporation leads to damage of the SAM and its interface with the substrate, ALD may become the technique of choice to establish the best metallic contacts on carboxylic acid terminated alkyl monolayers.

5. Conclusion

In summary, the present work shows that oxide-free carboxyl-terminated alkyl monolayers can be prepared free of electrical defects on hydrogenated silicon surfaces. The synthesis and preparation of these surfaces are compatible with the CMOS circuit fabrication and could therefore be used in microelectronics to tune the semiconductor properties and protect the interface. The SAM/silicon interface can be better controlled and is more stable when deposited directly on oxide-free silicon surfaces than on oxidized (SiO_2, Al_2O_3) or metallic surfaces (Al, Au). Moreover, the SAM layer is shown to protect the substrate from copper diffusion, as evident from the stability of Si−H and an absence of interfacial SiO_2 growth (i.e., < 5.6% ML). Copper is deposited on the SAM with less agglomeration than on typical oxide surfaces. The ALD method constitutes therefore an important first step to fabricate contacts on SAMs. Subsequent deposition using evaporation or other deposition methods can then complete the full deposition process. Indeed, the combined results from XPS and FTIR show that a primarily bidentate complexation occurs during the process. This configuration is associated with a gentle deposition of Cu and with a method that does not damage/penetrate the SAM or its interface with the substrate.

Acknowledgment. This work is supported by the National Science Foundation (Grant 0415652) and benefited from insightful discussions with Dr. Jinhee Kwon. We want to thank Prof. Roy Gordon for providing the Cu ALD precursor.

Supporting Information Available: Absorption spectra showing the Si−H mode at different steps of the SAM preparation, spectral expansion of the absorption spectrum shown in Figure 3c, normalized XPS spectra of C1s region of COOH-terminated SAM before and after 20 Cu ALD cycles, RBS thickness growth rate (per ALD cycle) of Cu films as a function of growth temperature on silicon oxide surfaces, and upper limits of oxidized silicon calculated from infrared absorption spectra and XPS spectra. This material is available free of charge via the Internet at http://pubs.acs.org.

JA907003W